CHEMPHYSCHEM

Supporting Information

Carotenoids as a Shortcut for Chlorophyll Soret-to-Q Band Energy Flow

Jan P. Götze,*[a] Dominik Kröner,[b] Shiladitya Banerjee,[b] Bora Karasulu,[a] and Walter Thiel[a]

cphc_201402233_sm_miscellaneous_information.pdf

1. Model system and computational details[1]

Starting from the PDB structure 2BHW,[2] the model system was built by including the following residues. From chain A: Val22-Phe28, Tyr44-Trp46, Phe189, Ala221-Phe228, chlorophyll-a residues 603, 604, and 608, and phosphatidylglycerol (LHG); from chain C: Trp128-Gln131, Gly136, chlorophyll-b residues 610 and 612, and diacylglycerol (DGD). For simplification, side chain groups were removed from Lys23 and Ser223 of chain A and from Ala129-Thr130 of chain C. Termini were capped by HCO- (N) or H2N-groups (C). Figure S 1 shows a pictorial representation of the model containing a total of 1,463 atoms.

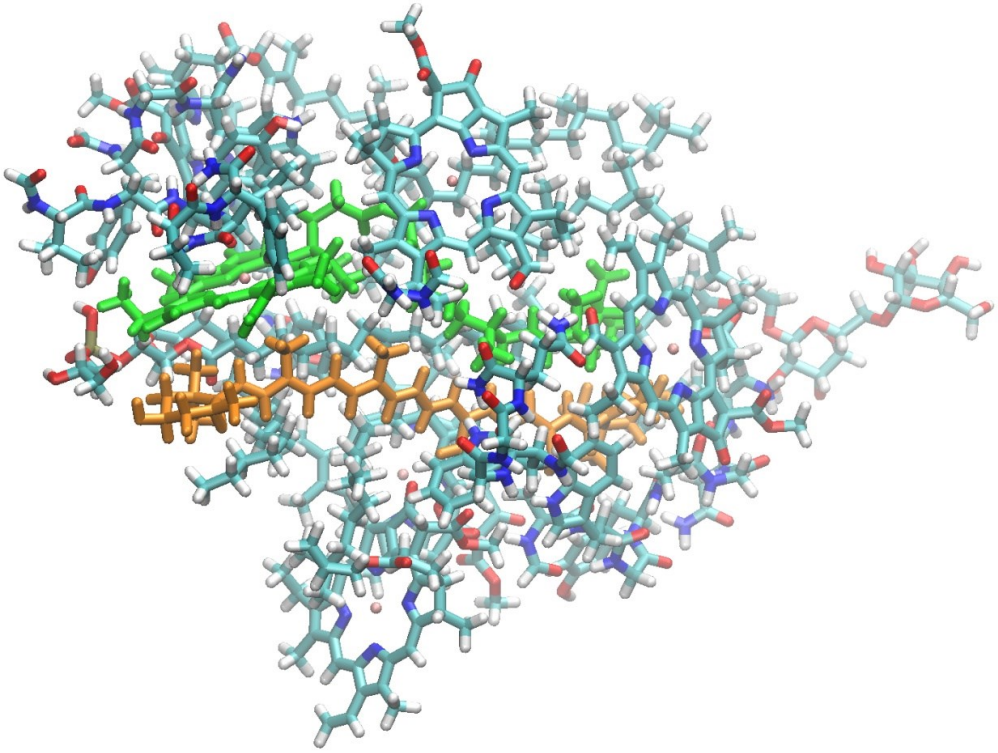

Figure S 1. Pictorial representation of the molecular model. Chlorophyll and xanthophyll residues of interest are highlighted in green and orange, respectively. Other atoms belong to the embedding shell.

The point charge field (PCF) was represented using RESP and Amber99[3] charges. It comprised the full LHCII crystal structure, as well as a thylakoid membrane slab provided by Bruce and Vassiliev.[4] Thylakoid membrane parts that overlapped with LHCII atoms were deleted. The PCF total charge was set to zero by adding sodium ions above and below the membrane slab, in an aqueous surrounding containing a total of 32,182 water molecules. More details can be found in Ref. [1].

As mentioned in the main text, the positions of the atoms were optimized prior to and in between spectral calculations. The PCF positions were adapted accordingly, with one exception: The changes in the DFT/MRCI Chl spectrum can be expected to be minute when using a different Vx or Zx geometry; consequently we omitted the update here to save computational effort.

2. Soret band orbital analysis

We state in the main article that the single-excitation composition of the Soret band states is different in the gas phase for DFT/MRCI and TD-DFT, while being fairly similar in the point charge field (PCF). The following analysis will support this statement, taking the case of Vx as an example.

Table S 1 shows the leading single excitations for each of the two energetically lowest Soret states. The associated orbitals are depicted in Figure S 2, Figure S 3 and Figure S 4. They are given simplified names to facilitate comparison and overview. Similar orbitals have identical names. Note that the "X4n" orbital in TD-DFT/PCF is mixing with a Vx orbital, and thus we have two "X4n" orbitals in that case.

Table S 1. CI vector components (TD-DFT) and determinant compositions (DFT/MRCI) for the Soret states presented in the main article. Only elements with squared coefficient of 0.05 or higher shown. Orbitals are given simplified designations; actual spatial plots and labels from a HOMO/LUMO scheme can be found in Figure S 2, Figure S 3, and Figure S 4.

TD-DFT, Vx/Chl, at ground state minimum geometry							
Gas phase				Point charge field			
Lower Soret state		Higher Soret state		Lower Soret state		Higher Soret state	
occ. -> virt.	coeff^2	occ. -> virt.	coeff^2	occ. -> virt.	coeff^2	occ. -> virt.	coeff^2
R4n -> R5n$^-$	0.59	X4n -> R5n$^-$	0.68	R4n -> R5n$^-$	0.54	X4n$^+$ -> R5n$^-$	0.35
X4n -> R5n$^+$	0.32	R4n -> R5n$^+$	0.22	X4n$^+$ -> R5n$^+$	0.16	R4n -> R5n$^+$	0.25
/	/	/	/	X4n$^-$ -> R5n$^+$	0.12	X4n$^-$ -> R5n$^-$	0.23
/	/	/	/	R4n -> R5n$^+$	0.05	R4n -> R5n$^-$	0.05
DFT/MRCI, Chl without phytyl, at ground state minimum geometry							
Gas phase				Point charge field			
Lower Soret state		Higher Soret state		Lower Soret state		Higher Soret state	
occ. -> virt.	coeff^2	occ. -> virt.	coeff^2	occ. -> virt.	coeff^2	occ. -> virt.	coeff^2
On$^+$ -> R5n$^-$	0.22	R4n -> R5n$^-$	0.22	R4n -> R5n$^-$	0.27	X4n -> R5n$^-$	0.22
R4n -> R5n$^-$	0.09	X4n -> R5n$^+$	0.11	X4n -> R5n$^+$	0.18	Exπ -> R5n$^+$	0.20
On$^+$ -> πn$^-$	0.07	X4n -> R5n$^-$	0.09	X4n -> R5n$^-$	0.14	R4n -> R5n$^+$	0.12
On$^+$ -> πn$^+$	0.07	On$^+$ -> R5n$^-$	0.08	R4n -> R5n$^+$	0.07	R4n -> R5n$^-$	0.05
On$^-$ -> R5n$^+$	0.06	Exπ -> R5n$^+$	0.06	/	/	/	/

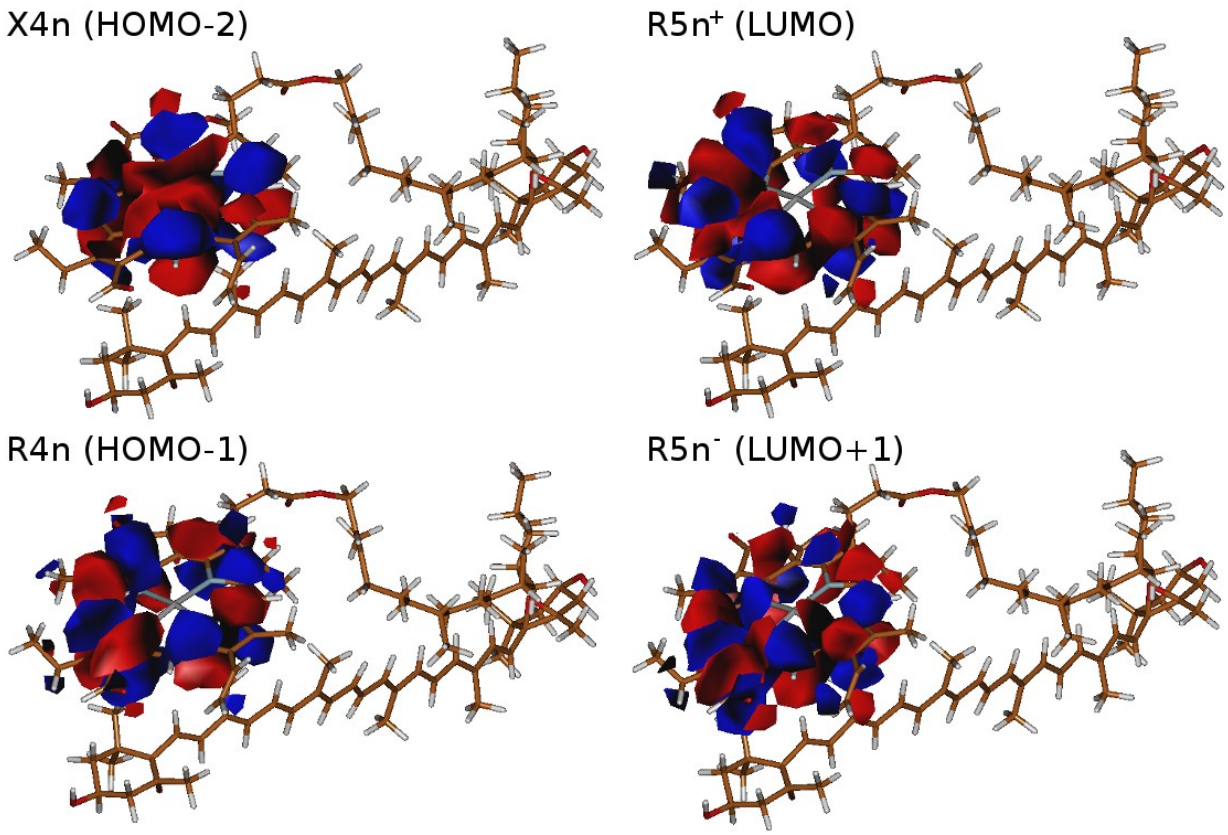

Figure S 2. Orbitals describing the two lowest Soret states for TD-DFT/gas phase, Vx/Chl; drawn at a contour value of 0.01

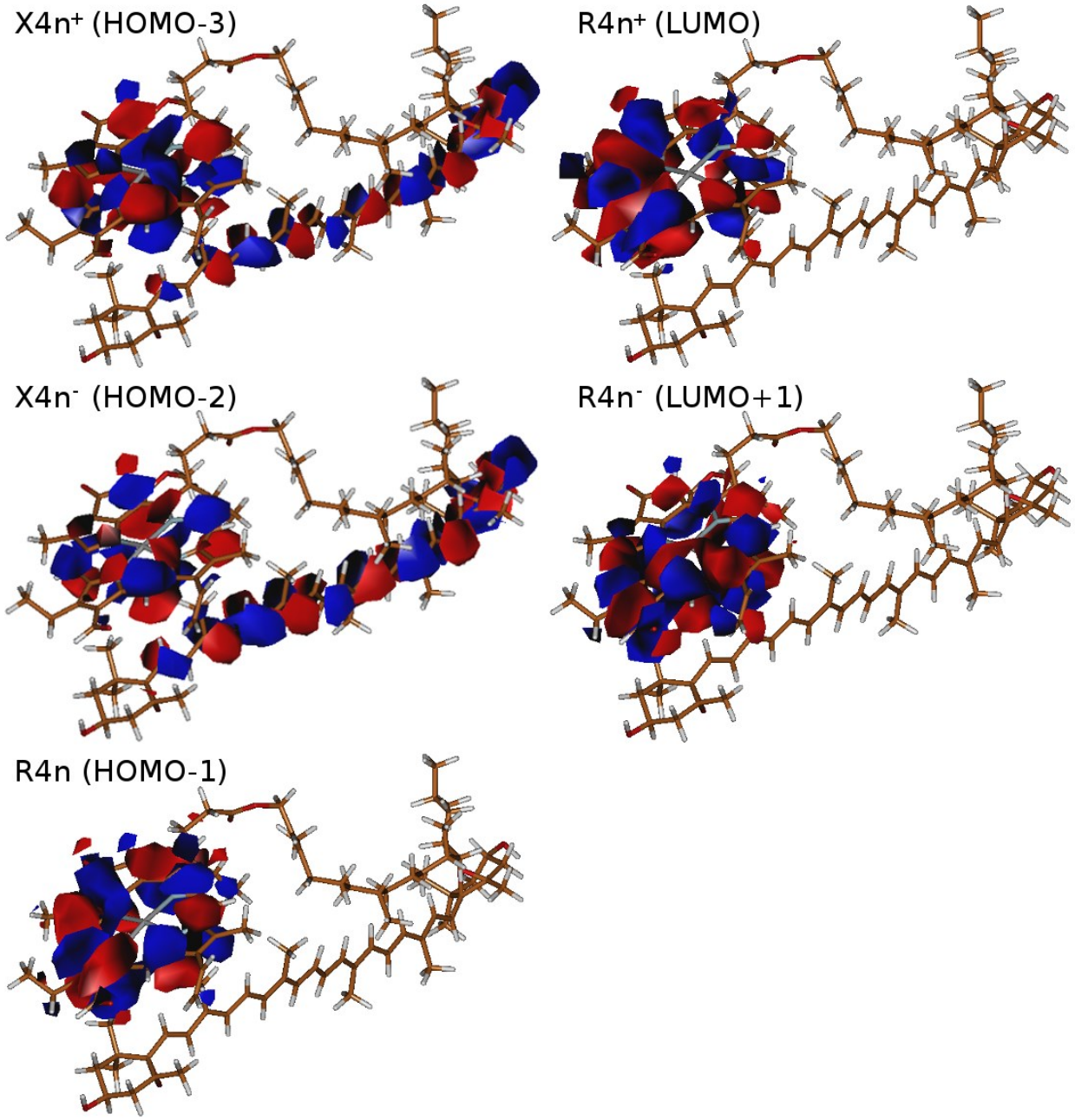

Figure S 3. Orbitals describing the two lowest Soret states for TD-DFT/PCF, Vx/Chl; drawn at a contour value of 0.01

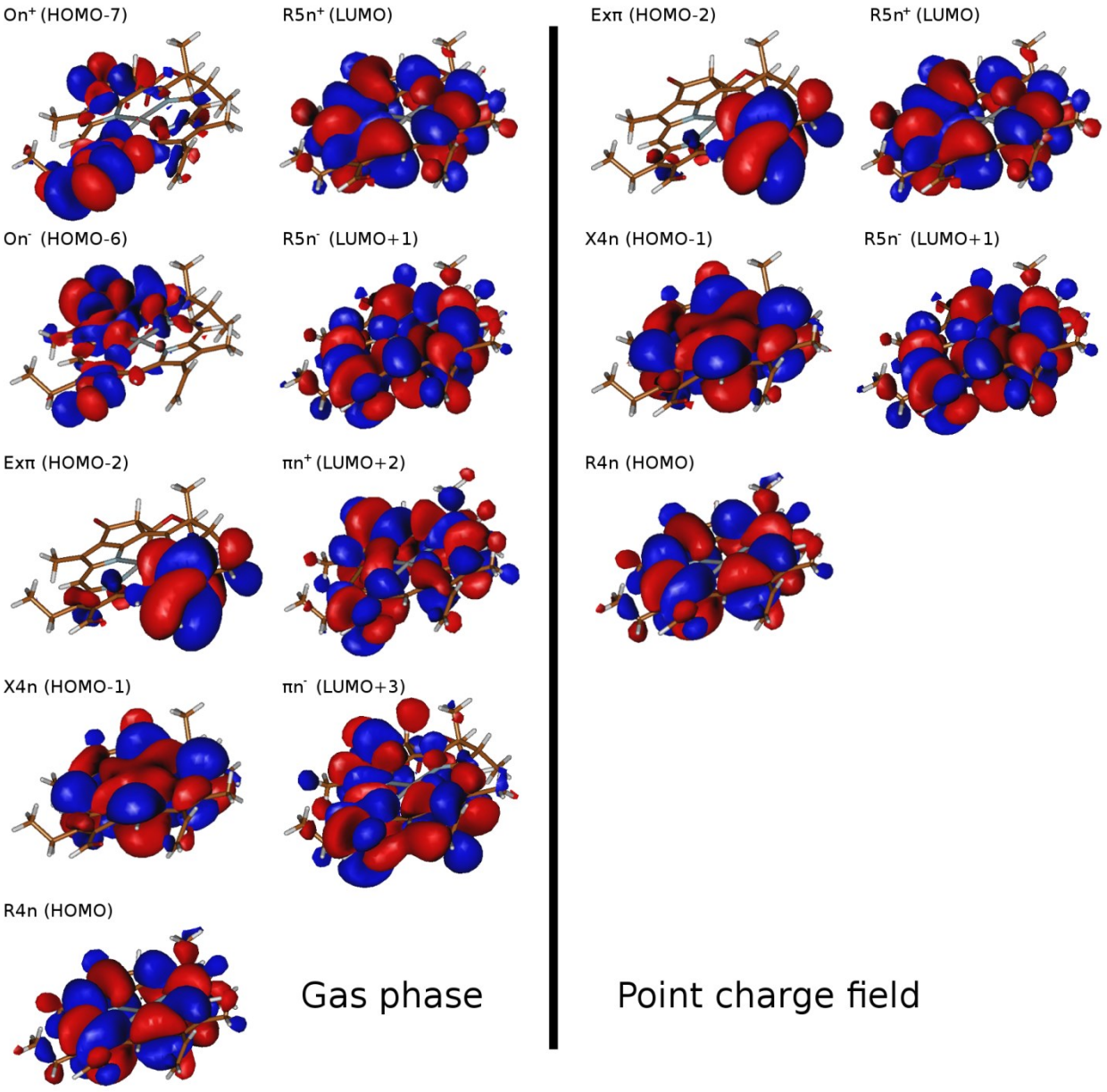

Figure S 4. Orbitals describing the two lowest Soret states for DFT/MRCI, Chl; drawn at a contour value of 0.01

In the PCF, the leading excitations are obviously identical for TD-DFT and DFT/MRCI (see Table S 1), even with partly similar weights (excluding the "Exπ" orbital, which is only present in the DFT/MRCI calculations). In the gas phase, however, the lower Soret state of TD-DFT is actually more similar to the higher Soret state of DFT/MRCI. There is no DFT/MRCI state among the calculated states that corresponds to the higher gas-phase TD-DFT Soret state, and no TD-DFT state that corresponds to the lower gas-phase DFT/MRCI Soret state. As a consequence, we cannot use the lower Soret state of DFT/MRCI (gas phase) for our PCF analysis, and we do not have a gas-phase energy of the higher DFT/MRCI Soret state in the PCF.

3. Vibrationally broadened Franck-Condon spectra for Vx and Zx in the protein environment

We computed the vibrationally broadened Franck-Condon (FC) spectra for Vx and Zx in the protein environment. We chose the time-independent approach to acquire a detailed spectral band structure, if required; we will however only present the convoluted spectra which would technically also have been available from a time-dependent FC calculation. The spectrum was computed using FCClasses,[5] interfaced to the DUSHIN program,[6] to allow for more choices of coordinate systems. The parameters for the computation at 0 K were up 10^9 integrals, a minimal Boltzmann weight of 0.0001, and a FWHM of 0.05 eV.

Due to the terminal ring structures, the relaxation of the excited state involves some significant rotational movement,[7] and therefore computation in Cartesian coordinates provided only minimal spectral yield (less than 0.02). The resulting spectral shapes are thus unreliable and not presented here. The use of curvilinear coordinates gave only slightly higher yields (Vx: 0.23, Zx: 0.07) indicating serious problems for standard FC spectra computation. One may thus expect the spectra to change upon more elaborate treatment (*e.g.*, including more integrals), but we did not find any significant changes in test calculations when tightening the parameters (see above) within a computationally affordable range. Given this situation we show the computed spectra here only for documentation (Figure S 5).

For Vx, the energetically lower band is underrepresented in the low-yield spectrum, while for Zx, the spectrum fits well to the experimental data. However, it needs to be emphasized that we computed the spectra at 0 K. At higher temperatures, there will be more transitions in the high-energy region, as can be seen by comparing to 77 K spectra.[8] Thus, the fact that the 0 K spectra compare so well to the 300 K experiment is likely a case of error compensation due to the low spectral yield.

The positions of the maxima and shoulders can be used to assess the accuracy of our computational methods. We compare to an experiment in acetone; as shown elsewhere, the introduction of a protein binding pocket leads to a systematic $1A_g \rightarrow 1B_u$ red shift of about 0.1 eV (for Vx).[1] Thus, we can conclude that the DFT/MRCI-corrected spectrum of Vx and Zx is of good quality,[9] while TD-CAM-B3LYP energies are blue-shifted (compared to DFT/MRCI) by 0.18 eV or 0.15 eV for Vx or Zx, respectively. A list of the approximate peak/shoulder maxima positions can be found in Table S 2.

Table S 2. Energies (in eV) of the predicted maxima/shoulders of the low-yield FC spectra for Vx and Zx.

	TD-DFT		DFT/MRCI-corr-TD-DFT		Experiment (Acetone)	
	Vx	Zx	Vx	Zx	Vx	Zx
Maximum 1	2.58	2.53	2.37	2.36	2.47	2.41
Maximum 2	2.74	2.71	2.54	2.54	2.67	2.58
Maximum/Shoulder 3	2.92	ca. 2.90	2.72	ca. 2.72	2.84	ca. 2.76

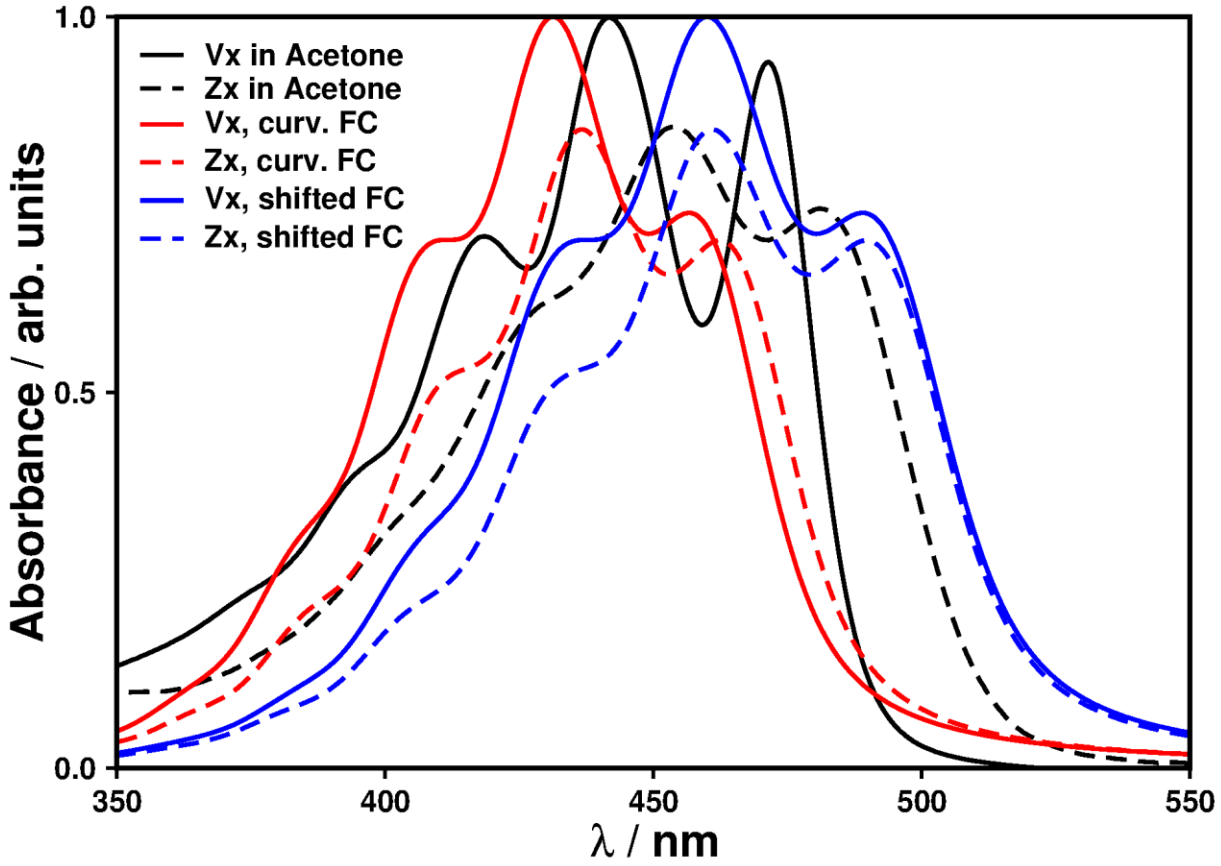

Figure S 5. Low-yield time-independent FC spectra of Vx (solid) and Zx (dashed). Spectral intensity normalized to maximum of the experimental spectrum in acetone (black, provided by Dr. Heiko Lokstein, Glasgow). Protein spectrum expected to be red-shifted by about 0.1 eV.[1] To obtain a FC spectrum for DFT/MRCI energies (blue),[9] the curvilinear FC spectra (red) were shifted by the DFT/MRCI minus TD-DFT vertical energies (Vx: -0.18 eV, Zx: -0.15 eV).

4. $1B_u/2A_g$ state mixing in the PCF

In the PCF, we find that the oscillator strengths (f) of $1A_g \rightarrow 2A_g$ rise at the cost of $f(1A_g \rightarrow 1B_u)$, despite the fact that the two states only getting slightly closer than in the gas phase, by 0.08 (Vx) or 0.05 (Zx) eV. The effect is most pronounced for Zx, where the two oscillator strengths in the PCF are found to be identical. We use this case as an example to show that the two states become similar in character in the PCF, except for their energetic positions, which remain well apart (see Table S 3).

Table S 3. Weights of the five leading DFT/MRCI configurations in the two lowest singlet excited states of Zx ($1A_g$ geometry)

Gas phase			
S_1: $2A_g$		S_2: $1B_u$	
Excitations	$coeff^2$	Excitations	$coeff^2$
$(HOMO \rightarrow LUMO)^2$	0.247	HOMO → LUMO	0.834
HOMO-1 → LUMO	0.158	HOMO-1 → LUMO+1	0.031
HOMO-1 + HOMO → LUMO + LUMO+1	0.138	HOMO-2 + HOMO → LUMO + LUMO+1	0.014
HOMO → LUMO+1	0.116	HOMO-1 + HOMO → LUMO + LUMO+2	0.011
Ground state	0.028	HOMO-1 + HOMO → LUMO	0.005
PCF			
S_1		S_2	
Excitations	$coeff^2$	Excitations	$coeff^2$
HOMO → LUMO	0.617	HOMO → LUMO	0.203
HOMO-1 + HOMO → LUMO + LUMO+1	0.063	HOMO-1 → LUMO	0.157
$(HOMO \rightarrow LUMO)^2$	0.057	HOMO → LUMO+1	0.129
HOMO-1 → LUMO+1	0.046	$(HOMO \rightarrow LUMO)^2$	0.088
HOMO-2 → LUMO	0.013	HOMO-1 + HOMO → LUMO	0.058

In the gas phase, the composition of the two lowest singlet states is as expected: the leading configurations for $2A_g$ and $1B_u$ are the HOMO → LUMO double and single excitations, respectively. In the PCF, symmetry is lost, and the two lowest states contain contributions from all kinds of excitations (including significant admixtures from the HOMO → LUMO single and double excitations in each case). This mixing leads to intensity borrowing and redistribution of oscillator strength. Going from the gas phase to the PCF, the character of the two lowest states changes in Zx: the energetically lower S_1 state in the PCF resembles the S_2 ($1B_u$) state in the gas phase, as can be seen from the weights of the HOMO → LUMO single excitation (0.617 vs. 0.834 compared with 0.203 in the PCF S_2 state). In the Vx case (see main article), the mixing does not increase as much when going from the gas phase to the PCF, and the oscillator strength of the S_1 state remains smaller than that of the S_2 state.

5. Optimizing a Vx/Chl pair in the $1B_u$ state

Optimizing both chromophores (Vx and Chl) together on the Vx $1B_u$ state surface requires more than 200 atoms to move along the TD-DFT excited-state gradient. With the chosen setup, the optimization ran for about six months (on a multiple-core machine) with several restarts. It did not finish in a proper minimum, presumably related to the fact that state crossings occur during the optimization. However, the course of the optimization and the concomitant changes in the character of the TD-DFT states allow for some additional insight into Chl/Vx coupling, which will be discussed in the following. A pictorial representation of the optimization path is given in Figure S 6, while the individual state composition is given in Table S 4 for selected points from Figure S 6.

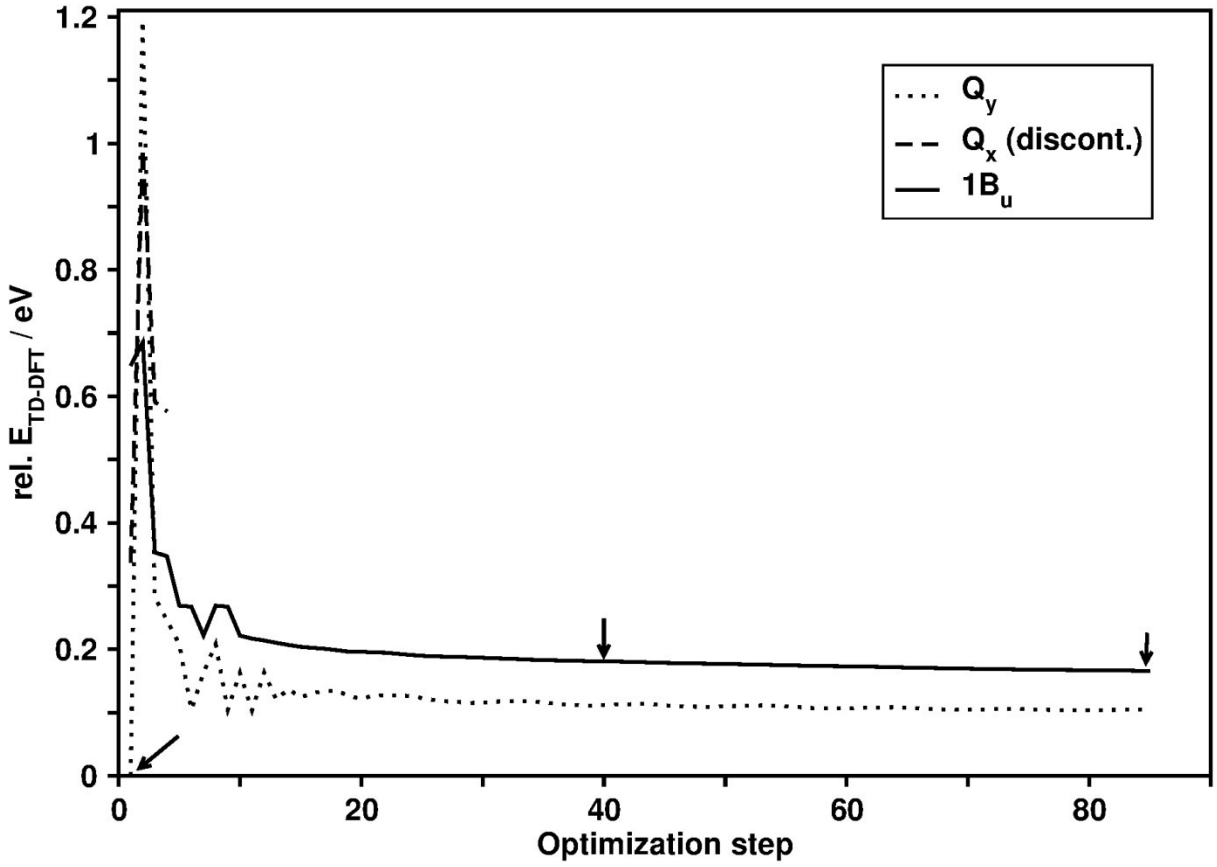

Figure S 6. TD-DFT energy minimization of a Vx/Chl pair in the ONIOM shell with both chromophores free to move on the $1B_u$ surface. The TD-DFT description of the marked points is documented in Table S 4 (first step, step 40, last step). The Q_x state was not followed further after few initial steps.

Table S 4. Single-excitation character of the Q_y and $1B_u$ states at selected points along the TD-DFT $1B_u$ optimization path (Figure S 6). Orbital labels of Chl according to Figure S 2.

First step			
Q_y		$1B_u$	
Excitations	coeff^2	Excitations	coeff^2
R4n → R5n$^+$	0.739	HOMO (XAT) → LUMO (XAT)	0.912
X4n → R5n$^-$	0.203	HOMO-1 (XAT) → LUMO+1 (XAT)	0.053
Step 40			
Q_y		$1B_u$	
Excitations	coeff^2	Excitations	coeff^2
R4n → R5n$^+$	0.683	HOMO (XAT) → LUMO (XAT)	0.854
X4n → R5n$^-$	0.160	R4n → R5n$^+$	0.071
HOMO (XAT)→ LUMO (XAT)	0.106	X4n → R5n$^-$	0.032
/	/	HOMO-1 (XAT) → LUMO+1 (XAT)	0.030
Last step (before crossing)			
Q_y		$1B_u$	
R4n → R5n$^+$	0.662	HOMO (XAT) → LUMO (XAT)	0.825
X4n → R5n$^-$	0.150	R4n → R5n$^+$	0.094
HOMO (XAT)→ LUMO (XAT)	0.136	X4n → R5n$^-$	0.038
/	/	HOMO-1 (XAT) → LUMO+1 (XAT)	0.028

Table S 4 shows that the mixing between the two states increases during the optimization (R4n → R5n$^+$ appears in $1B_u$, while HOMO (XAT) → LUMO (XAT) decreases; *vice versa* for Q_y). At the final point, the two states are less than 0.1 eV apart from each other, and the subsequent calculations fail to produce a proper excited-state gradient (causing termination of the run). These results would seem to support the possibility of a direct population transfer from the $1B_u$ state (at least of Vx) to Q_y.

References

[1] D. Kröner, J. P. Götze, *Journal of Photochemistry and Photobiology B: Biology* **2012**, *109*, 12-19.

[2] J. Standfuss, A. C. Terwisscha Van Scheltinga, M. Lamborghini, W. Kühlbrandt, *EMBO Journal* **2005**, *24*, 919-928.

[3] W. Wang, O. Donini, C. M. Reyes, P. A. Kollman, *Annu. Rev. Bioph. Biom.* **2001**, *30*, 211-243.

[4] a) S. Vassiliev, C. I. Lee, G. W. Brudvig, D. Bruce, *Biochemistry* **2002**, *41*, 12236-12243; b) S. Vassiliev, D. Bruce, *Photosynth. Res.* **2008**, *97*, 75-89; c) S. Vassiliev, P. Comte, A. Mahboob, D. Bruce, *Biochemistry* **2010**, *49*, 1873-1881.

[5] a) F. Santoro, R. Improta, A. Lami, J. Bloino, V. Barone, *Journal of Chemical Physics* **2007**, *126*, 084509; b) F. Santoro, A. Lami, R. Improta, V. Barone, *Journal of Chemical Physics* **2007**, *126*, 184102; c) F. Santoro, A. Lami, R. Improta, J. Bloino, V. Barone, *Journal of Chemical Physics* **2008**, *128*, 224311; d) V. Barone, J. Bloino, M. Biczysko, F. Santoro, *Journal of Chemical Theory and Computation* **2009**, *5*, 540-554; e) F. Santoro, *(available via the Internet at http://village.pi.iccom.cnr.it; last accessed 11. June 2012)* **2008**.

[6] J. R. Reimers, *Journal of Chemical Physics* **2001**, *115*, 9103-9109.

[7] J. P. Götze, W. Thiel, *Chemical Physics* **2013**, *415*, 247-255.

[8] D. M. Niedzwiedzki, J. O. Sullivan, T. Polívka, R. R. Birge, H. A. Frank, *Journal of Physical Chemistry B* **2006**, *110*, 22872-22885.

[9] D. Jacquemin, C. Adamo, *International Journal of Quantum Chemistry* **2012**, *112*, 2135-2141.